Non-Gaussian Model for Ringing Phenomena in Offshore Structures

Federico Waisman[1]; Kurtis Gurley, A.M.ASCE[2]; Mircea Grigoriu, M.ASCE[3]; and Ahsan Kareem, M.ASCE[4]

Abstract: Significant interest has been shown in identifying the nonlinear mechanisms that induce a ringing type response in offshore structural systems. This high frequency transient type response has been observed in offshore systems, particularly in tension leg platforms (TLPs). Given the implications of this behavior on the fatigue life of TLP tendons, it is essential that ringing be considered in the overall response evaluation. This study presents two non-Gaussian probabilistic models of nonlinear viscous hydrodynamic wave forces that induce ringing. The response of a single-degree-of-freedom system exposed to these non-Gaussian wave force models is then evaluated using analytical and numerical studies based on the Itô differentiation rule and the Monte Carlo simulation procedure, respectively. The results demonstrate that the proposed models induce ringing type response in a simplified structure. This study provides a probabilistic framework for modeling ringing type phenomenon which will serve as a building block for more refined hydrodynamic load models.

DOI: 10.1061/(ASCE)0733-9399(2002)128:7(730)

CE Database keywords: Offshore structures; Models; Gaussian process; Rings.

Introduction

The response of offshore platforms to wave forces occasionally exhibit sudden infrequent large magnitude bursts of short duration. This ringing behavior is distinctly different from the more commonly observed steady state springing response in the vertical and bending modes of tension leg platforms (TLPs) and gravity based structures (GBS) due to second-order wave effects at the sum frequencies. Ringing is the strong transient response observed in these modes triggered under severe loading conditions which decays to steady state at a rate that depends on the system damping. Both of these response types are delineated in Fig. 1.

The ringing response mechanism is not fully understood, making the incorporation of the ringing phenomenon in the reliability analysis of offshore platforms difficult. In recent years significant interest has been shown in identifying the wave mechanisms that induce ringing in complex offshore structural systems (Davies et al. 1994; Jeffreys and Rainey 1994; Natvig 1994; Faltinsen et al. 1995; Newman 1995; Chaplin et al. 1997; Gurley and Kareem 1998; Krokstad et al. 1998).

Gurley and Kareem (1998) conducted a numerical study in which it was shown that viscous type loading can induce ringing in an oscillating linear elastic single-degree-of-freedom (SDOF) cylinder piercing the water surface. The system parameters and wave conditions that are conducive to ringing were identified. The numerical simulations of wave forces employed by Gurley and Kareem (1998) are used to calibrate the probabilistic models in the current study. It is important to note that the nonlinear drag induced loading, obtained by integrating the sectional Morison force up to second order in wave elevation, is generally not believed to adequately explain the actual ringing phenomenon as observed in various applications, e.g., in large volume TLPs, where ringing is most clearly pronounced. For large volume structures a realistic modeling of the wave forces would include the additional contribution of nonslender-body terms (Chaplin et al. 1997; Krokstad et al. 1998). In this study, inertial force correction terms have not been included, and a small cylinder diameter/wavelength ratio is utilized with dominant viscous effects. Thus it must be stated that this study necessarily does not seek to emulate true TLP ringing response. The simplicity of the SDOF linear model and convenience of the nonlinear viscous loading to the free surface are applied to generate long time histories with characteristics that mimic observed ringing. The purpose of the study is the development of a probabilistic framework to represent such behavior, but not to identify the underlying causal mechanisms. A more complete study which seeks to accurately reflect the causes of ringing in a TLP would need to include a multi-degree-of-freedom (MDOF) system with both structural and geometric nonlinearities, explicit modeling of tendon dynamics, and a full description of known hydrodynamic loading mechanisms that incorporate both viscous and inertial loads as well as the effect of structural response on the loading. The fundamental probabilistic framework developed in this work could be extended to a multivariate version to model the behavior.

The objective of this study is to develop probabilistic models to represent the highly nonlinear and random transient features that closely resemble the ringing phenomenon. Based on this probabilistic format, more refined models of a realistic TLP system and hydrodynamic loading can be utilized to further advance the proposed methodology for large volume offshore platforms. Two models of the non-Gaussian wave state are developed, the

[1]Associate Product Line Manager/Catastrophe Peril, Swiss Re., 175 King St., Armonk, NY 10504.

[2]Assistant Professor, Dept. of Civil and Coastal Engineering, Univ. of Florida, Gainesville, FL 32611.

[3]Professor, School of Civil and Environmental Engineering, Cornell Univ., Ithaca, NY 14853.

[4]Professor, NatHaz Modeling Laboratory, Dept. of Civil Engineering and Geological Sciences, Univ. of Notre Dame, Notre Dame, IN 46556.

Note. Associate Editor: George Deodatis. Discussion open until December 1, 2002. Separate discussions must be submitted for individual papers. To extend the closing date by one month, a written request must be filed with the ASCE Managing Editor. The manuscript for this paper was submitted for review and possible publication on July 21, 2000; approved on January 2, 2002. This paper is part of the ***Journal of Engineering Mechanics***, Vol. 128, No. 7, July 1, 2002. ©ASCE, ISSN 0733-9399/2002/7-730–741/$8.00+$.50 per page.

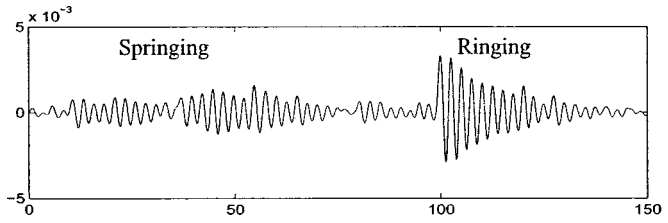

Fig. 1. Ringing and springing events

first is a superposition of a translation process (static transformation of a Gaussian process) and a Poisson white noise process which captures the infrequent bursts of energy in ringing inducing wave records. The second model is the sum of a filtered Poisson process and two Poisson white noise processes. Details concerning the calibration of these non-Gaussian models are described herein. The response of a simplified linear elastic SDOF offshore structure to the proposed wave loading models is conducted. In particular, when the second model is used, exact moments of any order of the response of linear elastic multi-degree-of-freedom structures can be found analytically based on the Itô differentiation rule. Furthermore, the second model can also be used to analytically obtain approximate moments of any order of the response of nonlinear systems by means of the Itô differentiation rule and a perturbation method (Waisman 1998; Waisman and Grigoriu 1998).

General of Wave Forces

Consider an oscillating cylindrical column of diameter D piercing the water surface as shown in Fig. 2. The SDOF linear elastic column oscillates to the passing waves about a fixed center of rotation c_r, which describes the location of the center of rotation with respect to the mean water level (denoted as $\otimes$ in Fig. 2). The draft, d_r, is the column length below the mean water level, and is always positive. The wave elevation $\eta(t)$ is positive above and negative below the mean water level. The depth d is set at 1,000 m.

The JONSWAP wave elevation spectrum is applied with a peak frequency of 0.1 Hz throughout this study. The literature survey indicates that the onset of ringing is triggered by a sudden large amplitude wave preceeded by a period of moderate wave activity. Large waves often exhibit an asymmetric wave profile which may lead to more favorable conditions for the onset of ringing. Asymmetry about the mean water level can be modeled by a second-order wave theory. In this study, Stokes second-order random waves are simulated utilizing a quadratic transfer function (QTF) in the Volterra series framework. The QTF is analytically derived based on Stokes second-order random wave (Hasselmann 1962; Hudspeth and Chen 1979; Kareem et al. 1994). Simulation details can be found in Gurley et al. (1996). The simulated realization of the surface elevation of gravity waves exhibit non-Gaussian features with characteristic high peaks and shallow troughs.

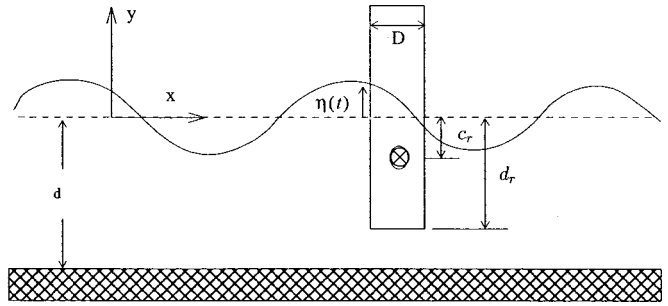

Fig. 2. SDOF model of cylinder in wave train

Application of the conventional description of the Morison equation to calculate the force at the mean water level ignores the nonlinear effects of the fluctuating free surface, which is thought to be a dominant ringing mechanism. In this study the wave kinematics up to the instantaneous water surface are used to generate moment input from both linear and second-order waves by integrating the force to the instantaneous free surface and multiplying by an equivalent moment arm. The water particle velocity at the mean water level is related to the velocity profile on the wetted cylinder using a modified Airy stretching theory (Mo and Moan 1985).

The drag force per unit length of the cylinder in Fig. 2 is

$$F_l(t)=\tfrac{1}{2}\rho C_d D u(t)|u(t)| \tag{1}$$

where ρ = fluid density, C_d = coefficient of drag, and $u(t)$ = instantaneous water particle velocity. The part of the cylinder below the mean water level is discretized in smaller segments. The portion below the mean water level and above the center of rotation is divided into *na* parts, and the portion below the center of rotation is divided into *nb* parts. The moment $M(t)$ produced by the drag forces on the cylinder is a combination of four components depending on the instantaneous wave elevation $\eta(t)$ with respect to the center of rotation and the mean water level (Gurley and Kareem 1998)

$$\begin{gathered}\eta(t)>0,\ \eta(t)>c_r,\ M(t)=M_1(t)+M_2(t)+M_3(t)\\ \eta(t)<0,\ \eta(t)>c_r,\ M(t)=M_2(t)+M_3(t)\\ \eta(t)<0,\ \eta(t)<c_r,\ M(t)=M_4(t)\end{gathered} \tag{2}$$

where the components $M_i(t),\ i=1,...,4$ are

$$M_1(t)=\frac{1}{2}\rho C_d D\eta(t)\left(\frac{\eta(t)}{2}-c_r\right)u_{\mathrm{mwl}}(t)|u_{\mathrm{mwl}}(t)| \tag{3}$$

$$M_2(t)=\sum_{i=1}^{na}\frac{1}{2}\rho C_d D u_i(t)|u_i(t)|d_l\left((na-i)d_l+\frac{d_l}{2}\right) \tag{4}$$

$$d_l=(n_l-c_r)/na,\quad n_l=\begin{cases}0, & \eta(t)>0\\ \eta(t), & \eta(t)\leqslant 0\end{cases}$$

$$M_3(t)=-\sum_{i=1}^{nb}\frac{1}{2}\rho C_d D u_i(t)|u_i(t)|d_l\left((i-1)d_l+\frac{d_l}{2}\right) \tag{5}$$

$$d_l=(d_r+c_r)/nb$$

$$M_4(t)=\sum_{i=1}^{nb}\frac{1}{2}\rho C_d D u_i(t)|u_i(t)|d_l\left((i-1)d_l+\frac{d_l}{2}-\eta(t)\right)$$

$$d_l=(d_r+\eta(t))/nb \tag{6}$$

in which $u_{\mathrm{mwl}}(t)$ = water particle velocity at the mean water level, $u_i(t)$ = local water velocity at the ith discrete portion of the cylinder, and d_l = length of the discretized section.

Records of the wave force moment $M(t)$ can be obtained by numerically simulating the wave elevation $\eta(t)$ and computing $M(t)$ from Eqs. (2)–(6). A set of 11 wave force moment records

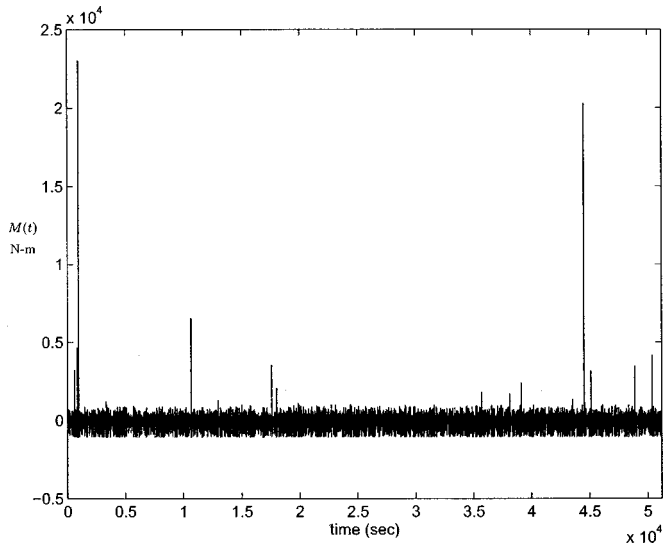

Fig. 3. Realization of $M(t)$

have been obtained from Gurley and Kareem (personal communications, 1997) in this study. One of these records is shown in Fig. 3.

Example of Nonlinear Wave Induced Ringing

An illustration of the onset of ringing in the numerical model used in this study is presented in Fig. 4 (Gurley and Kareem 1998). Figs. 4(a and b) show a Gaussian wave elevation train and the resulting cylinder response. No ringing event is observed. A second order contribution is then added to the same wave elevation train in Fig. 4(c). The resulting response in Fig. 4(d) shows that the nonlinear wave input triggers ringing while the linear wave input does not. The response to nonlinear waves is positively skewed due to the skewness in water particle velocity and has a high kurtosis around the transient ringing events due to the addition of extreme peak values in the response. Both the skewness and kurtosis lead to problems associated with extreme response and fatigue of ocean systems. It is noteworthy that not all large waves in the non-Gaussian wave train lead to ringing. A clearer

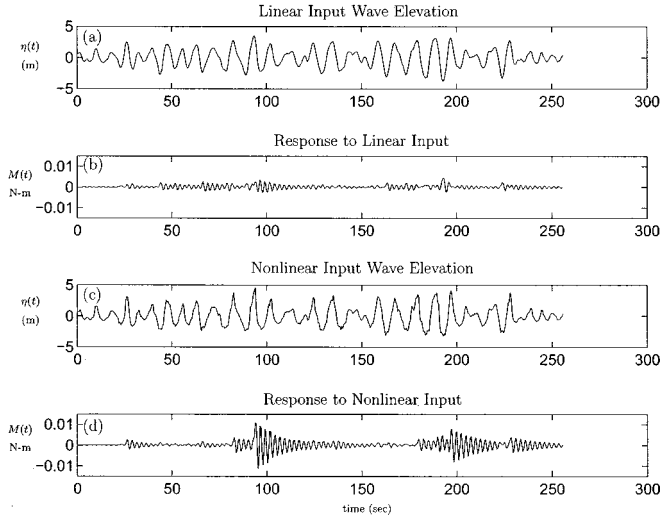

Fig. 4. Linear and nonlinear wave effects on system response

understanding of the mechanisms involved and its possible prediction have been the motivation for much work in recent literature. This study on the ringing phenomenon seeks to model the response using two different probabilistic approaches.

Probabilistic Models of Wave Forces

Let $M(t)=\{M_i, i=1,2,...,n\}$ be a time series of the input wave moment $M(t)$ at equal time intervals $\Delta t>0$. Fig. 3 shows a realization of this time series with $n=51, 200$ and $\Delta t=1$ s. The time series is characterized by large-amplitude infrequent short duration impulses. The time series $M(t)$ is decomposed into two time series, $M^c(t)$ and $M^i(t)$, such that

$$M(t)=M^c(t)+M^i(t) \tag{7}$$

where $M^c(t)$ represents the continuous component, and $M^i(t)$ the impulse component of M. The series $M^c(t)$ is obtained from $M(t)$ by removing the impulses present in the wave force record through a simple thresholding procedure. The series $M^i(t)$ contains the impulses removed from the continuous wave force record.

Two different wave force models are developed to represent the continuous and impulse components of $M(t)$. The first approach, referred to as the ''translation wave force model,'' represents the continuous component by a non-Gaussian translation process and the impulse component by a Poisson white noise process

$$X_T(t)=X_T^c(t)+X^i(t) \tag{8}$$

where X represents a model of M, the subscript $T=$translation model, the superscript $c=$continuous component, and the superscript $i=$impulse component.

The second approach, referred to as the ''filtered Poisson wave force model,'' represents the continuous component as the sum of a filtered Poisson and Poisson white noise processes, and the impulse component is the same Poisson white noise process used in Eq. (8)

$$X_F(t)=X_F^c(t)+X^i(t) \tag{9}$$

where the subscript $F=$sum of the filtered Poisson and Poisson white noise processes.

Eleven independent realizations of $M(t)$ of equal duration and time step as the record of Fig. 3 are used to estimate the parameters of the translation and filtered Poisson wave force models. The next three sections describe the modeling of the Poisson white noise impulse component and the translation and filtered Poisson continuous components.

Impulse Model $X^i(t)$

It is assumed that the impulses of the wave force process arrive in time according to a Poisson process. The validity of this assumption is verified by considering the time series realizations of $M^i(t)$, defined as

$$M^i(t)=\begin{cases} 0, & M(t)<2{,}000 \ \ N-m \\ M(t), & M(t)\geq 2{,}000 \ \ N-m \end{cases} \tag{10}$$

where the 2,000 $N-m$ threshold has been selected by visual inspection of the eleven independent realizations of $M(t)$ (Fig. 3).

Fig. 5(a) shows with a solid line the empirical distribution $\hat{F}_\tau$ of the interarrival times $\tau_i, i=1,...,90$, between consecutive impulses. The broken line in Fig. 5(a) is the distribution of an ex-

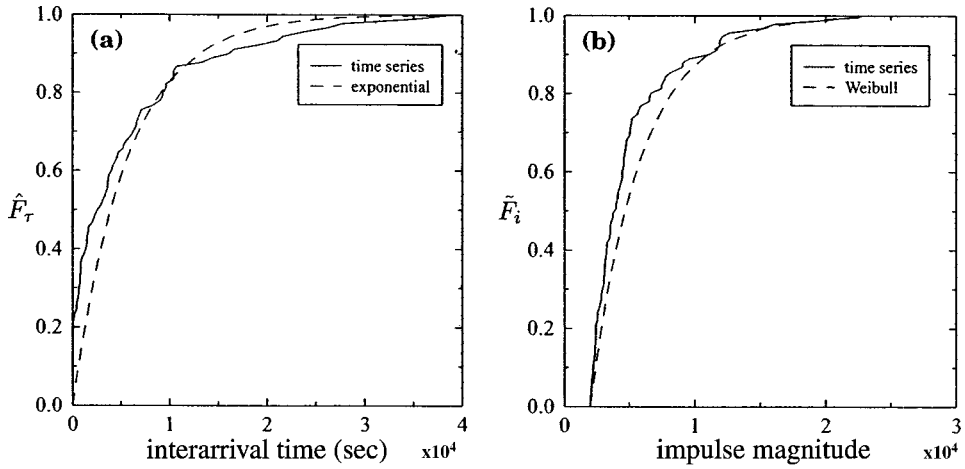

Fig. 5. Impulse model for M

ponentially distributed random variable with parameter $\hat{\lambda} = 1/E[\tau]$, where $E[\ ]$ is the expectation operator. The resulting average interarrival time between consecutive impulses $E[\tau]$ is 5,688 s, so that the estimate of the mean impulse arrival rate is $\hat{\lambda} = 0.000176$ arrivals/s. The agreement between the empirical data and the Poisson assumption model is satisfactory. Fig. 5(b) shows with a solid line the empirical distribution $\hat{F}_i$ of the impulses estimated from the set of eleven independent realizations of $M(t)$. This distribution was obtained using 91 impulses, and can be modeled by a Weibull distribution

$$\tilde{F}_i(x) = 1 - \exp\left(-\left[\frac{x - 2{,}000}{\alpha} \right]^c \right), \quad x \geq 2{,}000 \quad N - m \tag{11}$$

where $\alpha = 3883.79$ and $c = 1$, and is shown as the broken line in Fig. 5(b). The distributions have the same first and fourth central moment. The agreement between the empirical distribution and the model in Eq. (11) is satisfactory.

Translational Model of Continuous Component X_T^c

The first model of the continuous component consists of a translation of a Gaussian process into a non-Gaussian process. The spectrum of the underlying Gaussian process is selected such that the resultant non-Gaussian process has both the appropriate marginal probability distribution and power spectral density calibrated to match the empirical models' marginal probability distribution and power spectral density estimated from the continuous component of the wave forces M^c. The next three sections describe the estimation of the translation model parameters.

Let $\hat{F}_m$ be the empirical distribution of the continuous component M^c of the wave force process. Fig. 6 shows with a solid line this empirical distribution estimated from the set of 11 independent realizations of M. This empirical distribution is practically unchanged if the impulses of M are not eliminated from the record prior to estimation because they are very infrequent.

The model

$$\tilde{F}_m(x) = \begin{cases} 0.25 - 0.25\{1 - \exp[a_1(x + b_1)]\}, & x \leq -b_1 \\ 0.46 - 0.24[1 - \exp(a_2 x)], & -b_1 \leq x \leq 0 \\ 0.5 + 0.25[1 - \exp(-a_2 x)], & 0 \leq x \leq b_3 \\ 0.7 + 0.3\{1 - \exp[-a_3(x - b_3)]\}, & x \geq b_3 \end{cases} \tag{12}$$

of $\hat{F}_m$ with parameters $a_1 = 0.0031$, $a_2 = 0.02$, $a_3 = 0.0046$, $b_1 = 100$, and $b_3 = 80$ is shown with a broken line in Fig. 6. These parameters were obtained using a Marquard–Levenberg least-squares optimization procedure (Matlab 1998). The agreement between the empirical distribution and the model of Eq. (12) is satisfactory.

Fig. 7 shows with a solid line the ensemble averaged power spectral density $\hat{g}$ of the continuous component of the 11 independent realizations of M considered in the analysis. For every realization of M, its power spectral density is obtained by taking the inverse Fourier transform of its covariance function (Grigoriu 1995). The average of these 11 power spectral densities is $\hat{g}$ in Fig. 7. The figure shows that a significant fraction of the wave force energy is concentrated in the frequency range 0.06–0.14 Hz. Because the impulses of M occur very infrequently, the differences between the power spectral density of Fig. 7 and the one corresponding to the entire record M including the impulses are negligible.

Let $Y(t)$ be a stationary Gaussian process with mean μ_y defined by

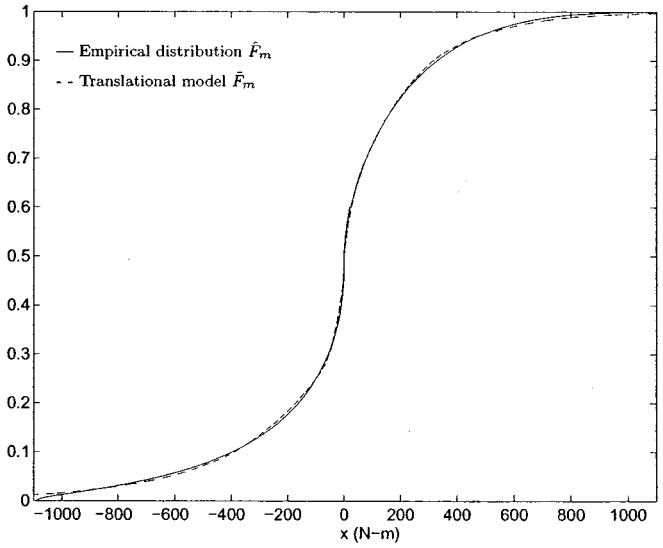

Fig. 6. Marginal distribution of $M^c(t)$

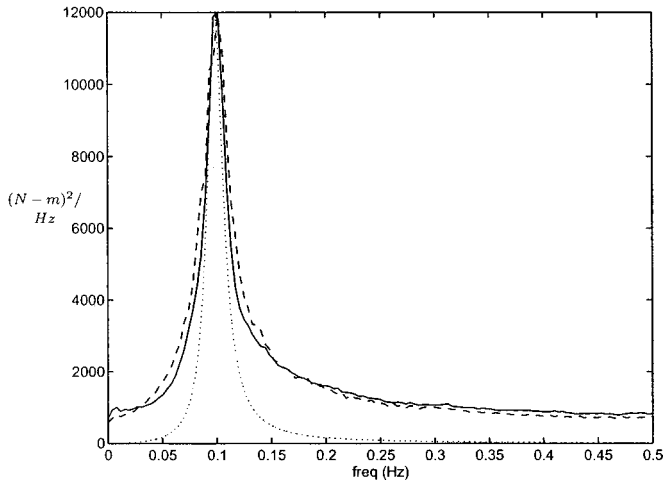

Fig. 7. Spectral densities of $M(t)$ (solid line $\hat{g}$), $Y(t)$ (dotted line $\tilde{g}$), and $X_T^c(t)$ (broken line $\tilde{g}_{X_T^c}$)

$$Y(t)=\mu_y+Z(t), \quad t\geq 0 \tag{13}$$

where $\{Z(t),t\geq 0\}$ is a stationary Gaussian process with mean zero and spectral density $\{\tilde{g}(f),f\in(0,0.5)\ \text{Hz}\}$ given by

$$\tilde{g}(f)=\frac{g_0(f/f_0)^2}{[1-(f/f_0)^2]^2+(2\zeta_0 f/f_0)^2} \tag{14}$$

The continuous component of the wave force process can be represented by the translation process

$$X_T^c(t)=\tilde{F}_m^{-1}\circ\Phi\left(\frac{Y(t)-\mu_y}{\sigma_y}\right)=g[Y(t)] \tag{15}$$

where σ_y = standard deviation of $Y(t)$ (Grigoriu 1995). The marginal distribution of X_T^c is $\tilde{F}_m$. The mean and correlation functions of this process are

$$\begin{aligned} E[X_T^c(t)]&=E\{g[Y(t)]\}\\ E[X_T^c(t)X_T^c(s)]&=E\{g[Y(t)]g[Y(s)]\}\end{aligned} \tag{16}$$

The parameters $g_0=388.8$, $f_0=0.098$ Hz, and $\zeta_0=0.565$ in Eq. (14) are selected through an iterative process such that the power spectral density $\tilde{g}_{X_T^c}$ of the translation process X_T^c in Eq. (15) matches the average power spectral density $\hat{g}$. Fig. 7 shows with a broken line the power spectral density $\tilde{g}_{X_T^c}$ of X_T^c for $\tilde{F}_m$ obtained numerically via a Monte Carlo simulation procedure and $\tilde{g}$ given by Eqs. (12) and (14), respectively. The graph of $\tilde{g}$ described in Eq. (14) is drawn as a dotted line in Fig. 7. The covariance function of Y is equal to $E[Z(t+\tau)Z(t)]$ so that the power spectral density of $Y(t)-\mu_y$ is $\tilde{g}(f)$ [Eq. (14)].

The resulting model X_T^c matches the marginal distribution and the correlation structure of the continuous component M^c of the wave force process. Therefore M^c can be approximated by X_T^c. The definition of the continuous component X_T^c of the wave force process can be modified by replacing the models $\tilde{F}_m$ and $\tilde{g}$ with the estimates $\hat{F}$ and $\hat{g}$, respectively. However, the use of the models $\tilde{F}_m$ and $\tilde{g}$ is more convenient for numerical calculations and they are used in this study.

Filtered Poisson Model of Continuous Component X_F^c

The second model of the continuous component M^c consists of the sum of a filtered Poisson component and a Poisson white noise component. The objective is to match the marginal distribution, correlation structure, and first four stationary moments of the continuous component M^c of the wave force process.

Let $X_F^c(t)=X_{F,0}^c(t)+X_{F,1}^c(t)$ be the continuous component of the wave force process, where $X_{F,0}^c(t)$ = filtered Poisson process and $X_{F,1}^c(t)$ = Poisson white noise process independent of $X_{F,0}^c(t)$. The component $X_F^c(t)$ is referred to as "Poisson model" and is an alternative model of $X_T^c(t)$. Both $X_F^c(t)$ and $X_T^c(t)$ are probabilistic models of the continuous component $M^c(t)$ of $M(t)$. The addition of the Poisson white noise process $X_{F,1}^c(t)$ is to match some moments of M^c.

The filtered Poisson process $X_{F,0}^c(t)$ is defined by

$$X_{F,0}^c(t)=\sum_{k=0}^{N_0(t)} Y_{k,0}h(t-\Gamma_{k,0}) \tag{17}$$

where $N_0(t),t\geq 0$ = homogeneous Poisson counting process of intensity $\lambda_0>0$, $\{Y_{k,0}\}$ = independent random variables with distribution F_0 arriving at random times $\{\Gamma_{k,0}\}$ of $N_0(t),t\geq 0$, and $h(t)$ = impulse response function. For this application, the impulse response function is defined by

$$h(t)=\begin{cases} 0, & t<0\\ \exp(-f_0c_0t)\sin(f_dt), & t\geq 0\end{cases} \tag{18}$$

where f_0 (rad/s) and c_0 = filter natural frequency and damping ratio, and $f_d=f_0\sqrt{1-c_0^2}$ (rad/s). The power spectral density of $X_{F,0}^c(t)$ is

$$\tilde{g}_0(f)=\frac{g_0}{(f^2-f_0^2)^2+(2c_0f_0f)^2}. \tag{19}$$

with $g_0=\lambda_0E[Y_{k,0}^2]/2\pi$.

The Poisson white noise process is defined by

$$X_{F,1}^c(t)=\sum_{k=0}^{N_1(t)} Y_{k,1}\delta(t-\Gamma_{k,1}) \tag{20}$$

where $N_1(t)$, $t\geq 0$ = homogeneous Poisson counting process of intensity $\lambda_1>0$, and $\{Y_{k,1}\}$ = independent random variables with distribution F_1 arriving at random times $\{\Gamma_{k,1}\}$ of $N_1(t)$, $t\geq 0$. The process power spectral density is

$$\tilde{g}_1(f)=g_1=\frac{\lambda_1E[Y_{k,1}^2]}{2\pi} \tag{21}$$

Fig. 8 shows with a solid line the average power spectral density $\hat{g}$ of the continuous component of the 11 independent realizations of M considered in the analysis. In the same figure with a broken line is shown the power spectral density of the continuous component $X_F^c(t)$, $\tilde{g}(f)=\tilde{g}_0(f)+\tilde{g}_1(f)$ with parameters $g_0=3.6e-6$, $f_0=0.1$ Hz, $\zeta_0=0.09$, and $g_1=0.15$.

Table 1 shows estimates of the first four stationary moments of the continuous component M^c of the 11 independent realizations of M.

The first four stationary central moments of the continuous component $X_F^c(t)$ are calculated analytically from Eq. (17) and the stationary moments of $X_{F,0}^c(t)$ and $X_{F,1}^c(t)$ as follows:

$$E[X_F^c(t)]=E[X_{F,0}^c(t)]+E[X_{F,1}^c(t)]=\mu_0+\mu_1=\mu \tag{22}$$

$$\begin{aligned} E([X_F^c(t)-\mu]^2)&=E([X_{F,0}^c(t)-\mu_0]^2)\\ &\quad+E([X_{F,1}^c(t)-\mu_1]^2)\end{aligned} \tag{23}$$

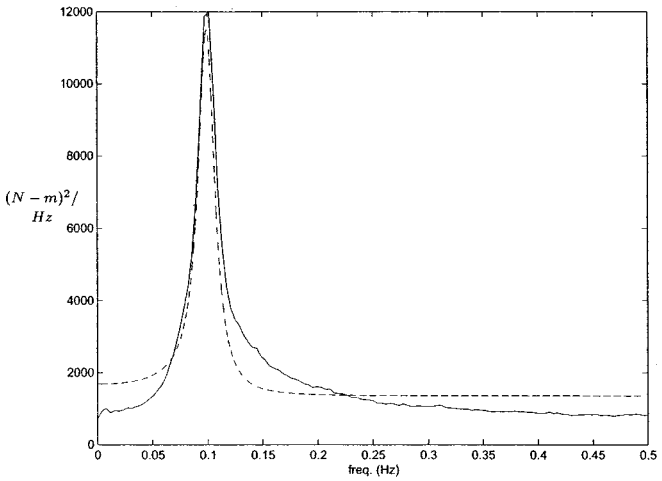

Fig. 8. Spectral densities of $M(t)$ (solid line) and $X_F^c(t)$ (broken line)

$$E([X_F^c(t)-\mu]^3)=E([X_{F,0}^c(t)-\mu_0]^3)+E([X_{F,1}^c(t)-\mu_1]^3) \tag{24}$$

$$E([X_F^c(t)-\mu]^4)=E([X_{F,0}^c(t)-\mu_0]^4)+E([X_{F,1}^c(t)-\mu_1]^4) \tag{25}$$

The moments of the filtered Poisson process $X_{F,0}^c(t)$ and the Poisson white noise process $X_{F,1}^c(t)$ are computed using cumulants (Grigoriu 1995; Waisman 1998; Waisman and Grigoriu 1998).

The objective is to match the first four stationary central moments of M^c with those of X_F^c. The parameters λ_0, λ_1, $E[Y_{k,0}^2]$, $E[Y_{k,1}^2]$, and the distributions F_0 and F_1 need to be defined for this purpose. Eq. (23) is already solved from the calculation of the power spectral densities in Fig. 8. It is assumed that the pulses $\{Y_{k,1}\}$ are Gaussian distributed with mean $\mu_{k,1}=-5.5e-3$ and variance $\sigma_{k,1}^2=2.95e-4$. It is also assumed that the pulses $\{Y_{k,0}\}$ are distributed according to a student's t distribution with probability density function (Johnson and Kotz 1970)

$$f_{Y_{k,0}}(y)=\frac{1}{\sqrt{\nu}B\left(\frac{1}{2},\frac{1}{2}\nu\right)}\left(1+\frac{y^2}{\nu}\right)^{-(1/2)(\nu+1)} \tag{26}$$

where $B=$ beta function and $\nu=$ degree of freedom of the distribution. This distribution is symmetric with respect to zero and as $\nu\to\infty$ the distribution tends to the standard normal distribution. The first four moments of $Y_{k,0}$ are

$$E[Y_{k,0}]=0$$

$$E[Y_{k,0}^2]=\frac{\nu}{\nu-2},\quad \nu\geq 2$$

$$\gamma_{3,0}=0 \tag{27}$$

Table 1. Stationary Moments of M^c

Statistics	M^c
$E[\cdot]$	-5.5×10^{-3}
Var$[\cdot]$	1.1667×10^{-2}
γ_3	-0.7146
γ_4	5.1206

$$\gamma_{4,0}=3+\frac{6}{\nu-4},\quad \nu\geq 4$$

Consider the transformation $Y_{k,0}^*=\gamma Y_{k,0}$, where $\gamma=$ constant. The variance of $Y_{k,0}^*$ is $\gamma^2E[Y_{k,0}^2]$ and the kurtosis is shown in Eq. (27). Thus the scaling of the first four moments of $\{Y_{k,0}\}$ reduces to the selection of the parameters γ and ν.

Based on a trial and error scheme, the remaining parameters were selected as $\lambda_0=10$, $\lambda_1=4$, $\gamma=1.4784e-4$, and $\nu=4.009193$, resulting in the following first moments of the continuous component $X_F^c(t)$:

$$E[X_F^c(t)]=\mu=-5.5e-3$$

$$E[X_F^c(t)-\mu]^2=1.0387e-2$$

$$\gamma_{3,X_F^c}=0$$

$$\gamma_{4,X_F^c}=5.1206 \tag{28}$$

The skewness coefficient is zero because the distributions F_0 (student's t) and F_1 (standard Gaussian) are symmetric and produce a poor match with the skewness of M^c. The resulting variance of $X_F^c(t)$ is slightly smaller than the variance of M^c, as can be seen in Fig. 8 and Table 1.

The resulting model X_F^c matches the correlation structure and three of the first four stationary moments of the continuous component M^c of the wave force process. Therefore M^c can be approximated by X_F^c.

Summary of Probabilistic Models of $M(t)$

The two probabilistic models of $M(t)$ are now summarized as

$$X_T(t)=X_T^c(t)+X^i(t) \tag{29}$$

and

$$X_F(t)=X_F^c(t)+X^i(t) \tag{30}$$

where

$$X_T^c(t)=\tilde{F}_m^{-1}\circ\Phi\left(\frac{Y(t)-\mu_y}{\sigma_y}\right),$$

$$X_F^c(t)=\sum_{k=0}^{N_0(t)}Y_{k,0}h(t-\Gamma_{k,0})+\sum_{k=0}^{N_1(t)}Y_{k,1}\delta(t-\Gamma_{k,1}) \tag{31}$$

$$X^i(t)=\sum_{k=1}^{N(t)}Y_k\delta(t-\tau_k)$$

with $h(t)$ defined in Eq. (18). The processes $X_T(t)$ and $X_F(t)$ are referred herein as the "translation wave force model" and "filtered Poisson wave force model," respectively. It should be noted that Eqs. (29) and (30) are the same as Eqs. (8) and (9). The impulse component $X^i(t)$ depends on a homogeneous Poisson counting process $N(t)$ with mean arrival rate $\hat{\lambda}$, the independent random variables $\{Y_k\}$ following the distribution $\tilde{F}_i$, the delta Dirac function δ, and the random times $\{\tau_k\}$ corresponding to the jumps of N. The impulses of the models $X_T(t)$ and $X_F(t)$ of the wave force processes are assumed to have no duration. The model of Eqs. (29) and (30) can be generalized to generate impulses of any specified shape. This extension can be achieved by replacing the Poisson white noise $\Sigma_{k=1}^{N(t)}Y_k\delta(t-\tau_k)$ in the definition of $X_T(t)$ and $X_F(t)$ by a filtered Poisson process. Results in this study are for the wave force models of Eqs. (29)–(31).

The response of an offshore structure modeled as a linear single-degree-of-freedom system to the translation and filtered Poisson wave force models is conducted. The analysis is based on analytical and numerical procedures using the Itô differentiation rule and the Monte Carlo simulation method, respectively.

Stochastic Differential Equations and the Itô Rule

The Itô differentiation rule provides a useful mathematical framework to obtain differential equations for functions of the solution of a stochastic differential equation. In this work the Itô differentiation rule is used to obtain moment equations of any order for the response of the linear offshore system subjected to the filtered Poisson processes. That is, the system response to the filtered Poisson wave force model will be determined via application of the Itô differential rule. The moment equations are exact and form a closed set of linear differential equations that can be solved by any conventional numerical method. Moreover, stationary moments can be obtained by solving linear algebraic equations.

Let $\{\mathbf{X}(t)\in\mathbb{R}^n, t\geqslant 0\}$ be the solution of the linear stochastic differential equation

$$d\mathbf{X}(t)=\mathbf{m}[\mathbf{X}(t),t]dt+\int_{\mathbb{R}^n}\mathbf{c}[\mathbf{X}(t),t,\mathbf{p}]M(dt,d\mathbf{p}),\quad t\geqslant 0 \tag{32}$$

where $\mathbf{m}(\mathbf{x},t)$ and $\mathbf{c}(\mathbf{x},t,\mathbf{p})=n$-dimensional and (n,m)-dimensional smooth functions, and $M(dt,d\mathbf{p})=$Poisson random measure (Gihman and Skorohod 1972; Snyder 1975; Ikeda and Watanabe 1981; Snyder and Miller 1991; Samorodnitsky and Taqqu 1994). The meaning of Eq. (32) is given by the integral form

$$\mathbf{X}(t)=\mathbf{X}(0)+\int_0^t\mathbf{m}[\mathbf{X}(s),s]ds+\int_0^t\int_{\mathbb{R}^n}\mathbf{c}[\mathbf{X}(s),s,\mathbf{p}]M(ds,d\mathbf{p}),\quad t\geqslant 0 \tag{33}$$

The first integral can be defined in the Riemann sense for every sample of $\mathbf{X}(t)$ because the process has continuous samples with probability one and the function $\mathbf{m}(x,t)$ is a smooth function. The second integral is a stochastic integral defined in the Itô sense (Gihman and Skorohod 1972; Snyder 1975; Ikeda and Watanabe 1981; Snyder and Miller 1991; Samorodnitsky and Taqqu 1994).

Existence and uniqueness of solution of Eqs. (32) and (33) plays an important role in determining the probabilistic characteristics of the solution $\mathbf{X}(t)$. For Poisson driven Markov processes three conditions need to be satisfied [Snyder and Miller (1991), Theorem 5.3.3, p. 256]: (i) $\mathbf{c}(\mathbf{x},t,\mathbf{p})$ is a continuous function of $\mathbf{x}$ and $\mathbf{p}$ and left continuous with respect to t; (ii) the functions $\mathbf{m}(\mathbf{x},t)$ and $\mathbf{c}(\mathbf{x},t,\mathbf{p})$ are Lipschitz continuous; and (iii) the function $\mathbf{c}(\mathbf{x},t,\mathbf{p})$ is bounded in the time-space rectangle of $[0,\infty)\times\mathbb{R}^n$ for every $\mathbf{x}$. The conditions (i) and (ii) guarantee the existence with probability one of the integral $\int_0^t\int_{\mathbb{R}^n}\mathbf{c}[\mathbf{X}(s),s,\mathbf{p}]M(ds,d\mathbf{p})$. The last condition assures the uniqueness of the solution $\mathbf{X}(t)$.

Itô Differentiation Rule

The Itô differentiation rule is used to obtain differential equations for any function of the stochastic vector process $\mathbf{X}(t)$ in Eqs. (32) and (33), provided that the function is continuous and twice differentiable. For example, by selecting an appropriate functional form, differential equations for the moments, characteristic function, Fokker–Planck equation, and Lyapunov exponents of $\mathbf{X}(t)$ can be obtained using the same mathematical tool: the Itô differentiation rule.

Let $g[\mathbf{X}(t),t]$ be a differentiable function and $\mathbf{X}(t)$ be the solution of Eqs. (32) and (33). The process $g[\mathbf{X}(t),t]$ is the solution of the stochastic integral equation (Gihman and Skorohod 1972; Snyder 1975; Ikeda and Watanabe 1981; Snyder and Miller 1991; Samorodnitsky and Taqqu 1994)

$$g[\mathbf{X}(t),t]=g[\mathbf{X}(0),0]+\int_0^t\left\{\frac{\partial g[\mathbf{X}(s),s]}{\partial s}+\sum_{k=1}^n m_k[\mathbf{X}(s),s]\times\frac{\partial g[\mathbf{X}(s),s]}{\partial X_k(s)}\right\}ds+\int_0^t\int_{\mathbb{R}^n}\{g[\mathbf{X}(s)+\mathbf{c}[\mathbf{X}(s),s,\mathbf{p}],s]-g[\mathbf{X}(s),s]\}M(ds,d\mathbf{p}) \tag{34}$$

with differential form

$$dg[\mathbf{X}(t),t]=\left\{\frac{\partial g[\mathbf{X}(t),t]}{\partial t}+\sum_{k=1}^n m_k[\mathbf{X}(t),t]\frac{\partial g[\mathbf{X}(t),t]}{\partial X_k(t)}\right\}dt+\int_{\mathbb{R}^n}\{g[\mathbf{X}(t)+\mathbf{c}[\mathbf{X}(t),t,\mathbf{p}],t]-g[\mathbf{X}(t),t]\}\times M(dt,d\mathbf{p}) \tag{35}$$

Any vector $\mathbf{X}(t)$ satisfying a stochastic differential equation of the type of Eqs. (32) and (33) and the Itô differentiation rules of Eqs. (34) and (35) can be used to develop differential equations for differentiable functions of this vector. This observation and the differentiable function in Eq. (36), depending on the components of $\mathbf{X}(t)$ and positive integers $\{q_i\}$, can be used to develop differential equations for the moments of $\mathbf{X}(t)$.

$$g[\mathbf{X}(t)]=\prod_{i=1}^n X_i(t)^{q_i} \tag{36}$$

Response Analysis

The response of an offshore structure modeled as a linear system to the two probabilistic models of the wave force processes $X_T(t)$ [Eq. (29)] and $X_F(t)$ [Eq. (30)] is performed. Numerical and analytical studies are carried out based on the Monte Carlo simulation method and the Itô differentiation rule, respectively. Validation of the probabilistic models is conducted through comparison of system response to the original wave forces and the response to the translation and filtered Poisson wave force models, respectively.

Consider an offshore structure modeled as a single-degree-of-freedom linear system with moment of inertia m, damping c, and stiffness k defined by

$$m\ddot{\Theta}(t)+c\dot{\Theta}(t)+k\Theta(t)=M(t) \tag{37}$$

where $\Theta(t)=$rotation about the horizontal axis perpendicular to incoming waves, and $M(t)=$wave force process representing the instantaneous moment acting on a cylindrical column piercing the water surface. Fig. 9 shows the system response $\Theta(t)$ subjected to the wave force record shown in Fig. 3, for $m=2{,}876.88$, $c=181.73$, and $k=18173.23$. These structural parameters were

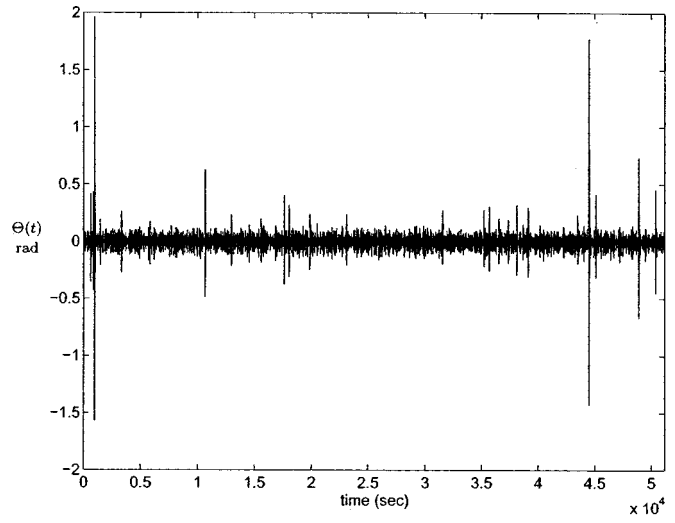

Fig. 9. System response $\Theta(t)$ to the realization of $M(t)$ in Fig. 3

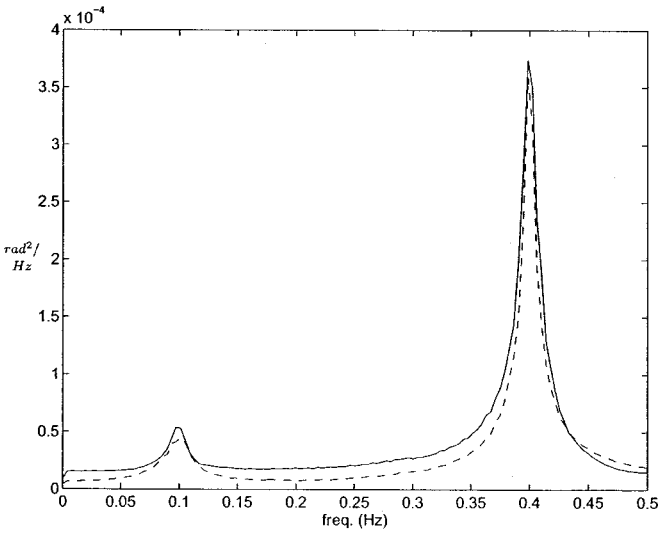

Fig. 11. Power spectral densities of $\Theta(t)$ (solid line) and $\tilde{\Theta}_T(t)$ (broken line)

chosen to impart a convenient natural period for the oscillator to induce ringing-like behavior, and do not reflect the values for a particular physical structure.

Response Analysis to Translation Wave Force Model $X_T(t)$

Let $\tilde{\Theta}_T(t)$ be the solution of

$$m\ddot{\tilde{\Theta}} + c\dot{\tilde{\Theta}}_T(t) + k\tilde{\Theta}_T(t) = X_T(t) \tag{38}$$

where $X_T(t)$ is given by Eqs. (29) and (31). Let Θ_T^c and Θ^i = stationary responses of the linear system of Eq. (38) to X_T^c and X^i, respectively. Then, the response to the wave force model $X_T(t)$ is $\tilde{\Theta}_T(t) = \tilde{\Theta}_T^c(t) + \tilde{\Theta}^i(t)$. Fig. 10(a) shows the system response $\tilde{\Theta}_T(t)$ of Eq. (38) to a sample of the wave force process $X_T(t) = X_T^c(t) + X^i(t)$. Fig. 10(b) shows in more detail the ringing phenomena in the response $\tilde{\Theta}_T$ around time $t = 5{,}400$ s where the transient response associated with a ringing event can be observed clearly and resembles Fig. 1. The subsequent decay rate depends on the system damping.

The response analysis of Eq. (38) is performed in three steps. First, the theory of filtered Poisson processes is used to find analytically the response component $\tilde{\Theta}^i(t)$ to the input impulses $X^i(t)$ defined by Eq. (31). Second, the Monte Carlo simulation is used to calculate realizations of the response component $\tilde{\Theta}_T^c(t)$ to the input $X_T^c(t)$ defined by Eq. (31). Third, the total response $\tilde{\Theta}_T(t)$ as shown in Fig. 10(b) is defined by the superposition $\tilde{\Theta}_T(t) = \tilde{\Theta}_T^c(t) + \tilde{\Theta}^i$.

Fig. 11 shows the power spectral densities of $\Theta(t)$ and $\tilde{\Theta}_T(t)$. The solid line is the power spectral density of the response $\Theta(t)$ of the system in Eq. (37) to the 11 independent realizations of $M(t)$. The broken line in Fig. 11 is the power spectral density of $\tilde{\Theta}_T(t)$ of the response of Eq. (38) to the translation wave model obtained via Monte Carlo simulation in conjunction with spectrum estimation. The power spectral densities have two distinct peaks, located at 0.1 and 0.4 Hz, corresponding to the wave force energy content and the oscillator natural frequencies, respectively. The agreement between the response of the system in Eq. (37) to the empirical data and the proposed model is satisfactory.

Fig. 12 shows with a solid line the empirical marginal distribution of the solution $\Theta(t)$ of Eq. (37). The empirical marginal

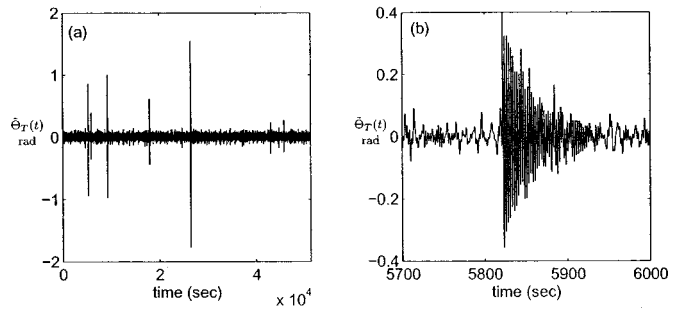

Fig. 10. System response $\tilde{\Theta}_T(t)$ to a sample of $X_T(t)$

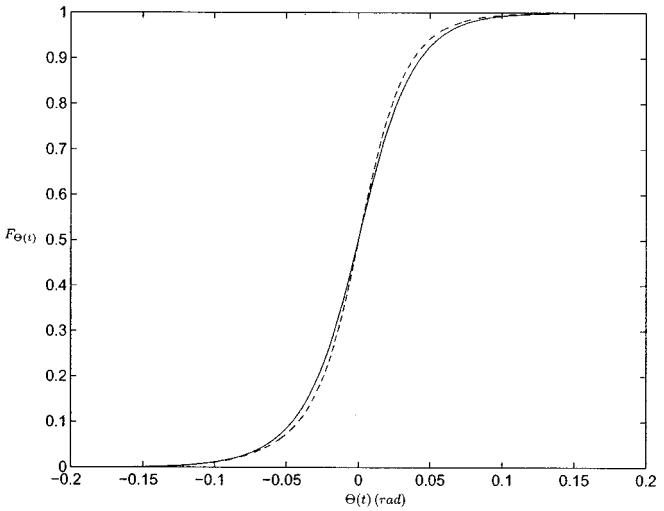

Fig. 12. Marginal distribution of $\Theta(t)$ (solid line) and $\tilde{\Theta}_T(t)$ (broken line)

Table 2. Stationary Response Moments for the Translational Model $X_T(t)$

Statistics	$\Theta(t)$	$\tilde{\Theta}_T(t)$
$E[\cdot]$	-8.34×10^{-4}	8.24×10^{-4}
Var$[\cdot]$	0.0020	0.0019
γ_3	0.6772	0.7142
γ_4	88.9081	99.8921

distribution of the response $\tilde{\Theta}_T(t)$ of the linear system to the proposed model is shown with a broken line in Fig. 12. A good agreement is noted.

Table 2 shows that the stationary first four moments of the system responses $\Theta(t)$ and $\tilde{\Theta}_T(t)$ are in very good agreement, indicating a good match in Fig. 12.

Response Analysis to Poisson Wave Force Model $X_F(t)$

Let $\tilde{\Theta}_F$ be the solution of

$$m\ddot{\tilde{\Theta}}_F(t)+c\dot{\tilde{\Theta}}_F(t)+k\tilde{\Theta}_F(t)=X_F(t) \tag{39}$$

where $X_F(t)$ is given by Eqs. (30) and (31) and consists of a superposition of two Poisson white noises processes $[X^c_{F,1}(t)$ and $X^i(t)]$ and a filtered Poisson process $[X^c_{F,0}(t)]$. Based on this, the linear system in Eq. (39) can be written as

$$\ddot{\tilde{\Theta}}_F(t)+c/m\dot{\tilde{\Theta}}_F(t)+k/m\tilde{\Theta}(t)_F=[X^c_{F,0}(t)+X^c_{F,1}(t)+X^i(t)]/m \tag{40}$$

$$\ddot{X}^c_{F,0}(t)+2c_0f_0\dot{X}^c_{F,0}(t)-f_0^2X^c_{F,0}(t)=1/m\sum_{k=0}^{N_0(t)}Y_{k,0} \tag{41}$$

where the right-hand side of Eq. (41) is the Poisson white noise driving $X^c_{F,0}$ in Eq. (17).

The augmented state vector $\mathbf{\Theta}(t)=\{\tilde{\Theta}(t)_F,\dot{\tilde{\Theta}}_F(t),X^c_{F,0}(t),\dot{X}^c_{F,0}(t)\}'$ is the solution of the stochastic differential equation [Eqs. (40) and (41)]

$$d\begin{bmatrix}\tilde{\Theta}_F(t)\\ \dot{\tilde{\Theta}}_F(t)\\ X^c_{F,0}(t)\\ \dot{X}^c_{F,0}(t)\end{bmatrix}=\begin{bmatrix}\dot{\tilde{\Theta}}_F(t)\\ -c/m\dot{\tilde{\Theta}}_F(t)-k/m\tilde{\Theta}_F(t)+X^c_{F,0}(t)/m\\ \dot{X}^c_{F,0}(t)\\ -2c_0f_0\dot{X}^c_{F,0}(t)-f_0^2X^c_{F,0}(t)\end{bmatrix}dt+\begin{bmatrix}0\\ \frac{\sqrt{\pi g_1}}{m}\\ 0\\ 0\end{bmatrix}\sum_{k=0}^{N_1(t)}Y_{k,1}+\begin{bmatrix}0\\ 0\\ \frac{\sqrt{\pi g_i}}{m}\\ 0\end{bmatrix}\sum_{k=0}^{N(t)}Y_k+\begin{bmatrix}0\\ 0\\ \hat{0}\\ 1/m\end{bmatrix}\sum_{k=0}^{N_0(t)}Y_{k,0} \tag{42}$$

where $g_i=\hat{\lambda}E[Y_k^2]/2\pi$ is the power spectral density of the Poisson white noise process X^i representing the impulsive component M^i of M.

Because the augmented state vector $\mathbf{\Theta}(t)$ of Eq. (42) satisfies a stochastic differential equation of the type of Eqs. (32) and (33), the Itô differentiation rules of Eqs. (34) and (35) and the differentiable function in Eqs. (36) are used to develop differential equations for the moments of $\mathbf{\Theta}(t)$. The moments $\mu(p,q,r,s;t)=E[\tilde{\Theta}_F(t)^p\dot{\tilde{\Theta}}_F(t)^qX^c_{F,0}(t)^r\dot{X}^c_{F,0}(t)^s]$ are obtained by applying Eqs. (35) and (36), ensemble averaging, and dividing by dt. Details of this procedure can be found in Waisman (1998). These equations are

$$\begin{aligned}\dot{\mu}(p,q,r,s;t)=&-(k/mq+2c_0f_0s)\mu(p,q,r,s;t)+p\mu(p-1,q+1,r,s;t)-k/mq\mu(p+1,q-1,r,s;t)+q\mu(p,q-1,r+1,s;t)\\&+r\mu(p,q,r-1,s+1;t)-f_0^2s\mu(p,q,r+1,s-1;t)+\frac{\hat{\lambda}}{m}\sum_{j=1}^{q}\frac{q!}{j!(q-j)!}\mu(p,q-j,r,s;t)E[Y_k^j]\\&+\frac{\lambda_0}{m}\sum_{j=1}^{q}\frac{q!}{j!(q-j)!}\mu(p,q-j,r,s;t)E[Y_{k,0}^j]+\frac{\lambda_1}{m}\sum_{j=1}^{s}\frac{s!}{k!(s-j)!}\mu(p,q,r,s-j;t)E[Y_{k,1}^j]\end{aligned} \tag{43}$$

The set of equations generated by Eq. (43) is closed, and thus it can be solved exactly based on three observations: (1) the moments $\mu(0,0,0,s;t)$ of any order s can be calculated exactly because they correspond to the filtered Poisson process $X_F(t)$ (Grigoriu 1995); (2) the moments $\mu(p,q,r,s;t)$ vanish if one or more arguments are strictly smaller than zero; and (3) the set of moment equations of order $p+q+r+s$ generated by Eq. (43) involve the moments of order $p+q+r+s$ or lower. There is no need to use closure techniques for solution. Initial conditions are needed for solving Eq. (43) and these conditions need to be specified. If the coefficients of the differential equation defining $\mathbf{\Theta}(t)$ are time invariant and $\mathbf{\Theta}(t)$ becomes stationary as $t\to\infty$, the moments $\mu(p,q,r,s;t)=\mu(p,q,r,s)$ do not depend on time so that $\dot{\mu}(p,q,r,s;t)=0$ in Eq. (43). In this case, the moments of $\mathbf{\Theta}(t)$ are the solution of algebraic equations.

Fig. 13 shows the evolution in time of the mean, variance, skewness, and kurtosis coefficients of $\tilde{\Theta}_F(t)$ corresponding to the initial conditions $\mathbf{\Theta}(t)=\mathbf{0}$.

The agreement between the stationary values of the mean, variance, and coefficient of kurtosis with the corresponding measures from the 11 independent wave force records of $M(t)$ is satisfactory. There is a mismatch, however, with the coefficient of

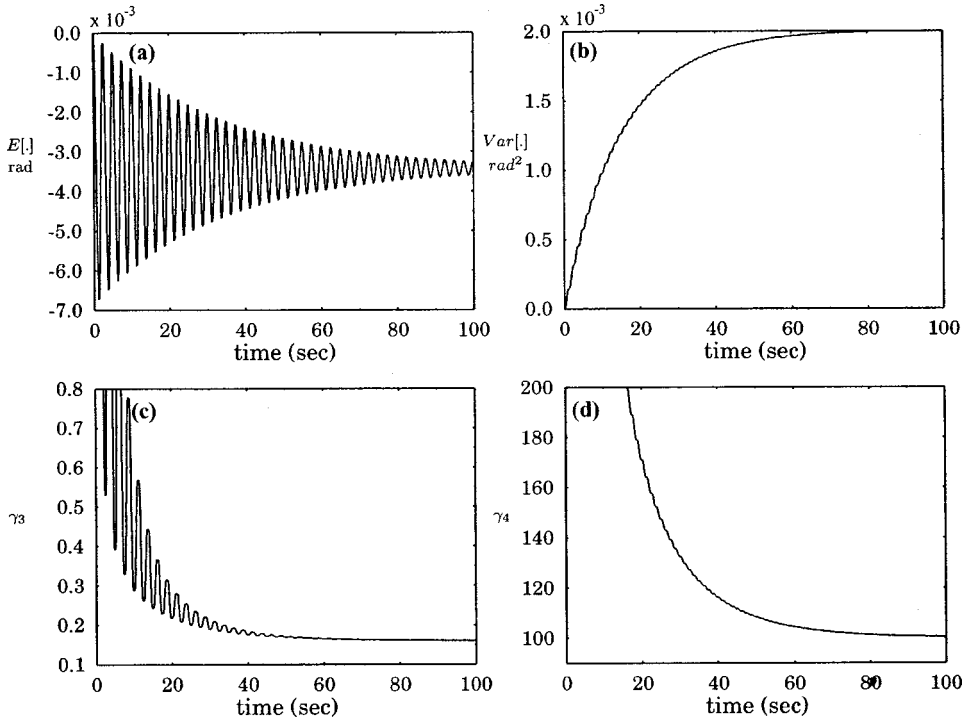

Fig. 13. Exact moments of the response $\tilde{\Theta}_F(t)$: (a) mean; (b) variance; (c) coefficient of skewness; and (d) coefficient of kurtosis

skewness. This behavior was expected due to the fact that the marginal distributions selected for the filtered Poisson wave force model where symmetrical ($\gamma_3=0$).

Let $\Theta^c_{F,0}(t)+\Theta^c_{F,1}(t)$ and $\Theta^i(t)$ be the stationary responses of the linear system of Eq. (39) to $X^c_{F,0}(t)+X^c_{F,1}(t)$ and $X^i(t)$, respectively. Then, the response to the wave force model $X_F(t)$ is $\tilde{\Theta}_F(t)=\tilde{\Theta}^c_{F,0}(t)+\tilde{\Theta}^c_{F,1}(t)+\tilde{\Theta}^i(t)$. Fig. 14(a) shows the system response $\tilde{\Theta}_F(t)$ of Eq. (39) to a sample of the wave force process $X_F(t)=X^c_{F,0}(t)+X^c_{F,1}(t)+X^i(t)$. Fig. 14(b) shows in more detail the ringing phenomena on the response $\tilde{\Theta}_F$ of Eq. (39). This figure details the response of Fig. 14(a) around time $t=5{,}800$ s. The transient response associated with a ringing event can be observed clearly and resembles Fig. 1. The decay rate depends on the system damping.

The response analysis of Eq. (39) is performed in three steps. First, the theory of filtered Poisson processes is used to find analytically the response components $\Theta^c_{F,1}(t)$ and $\tilde{\Theta}^i(t)$ to the inputs $X^c_{F,1}(t)$ and $X^i(t)$ defined by Eq. (31), and the input process $X^c_{F,0}(t)$ using Eqs. (17) and (18). Second, the Monte Carlo simulation is used to calculate realizations of the response component $\tilde{\Theta}^c_{F,0}(t)$ to the input $X^c_{F,0}(t)$ computed in the previous step. Third, the total response $\tilde{\Theta}_F(t)$ as shown in Fig. 14(a) is defined by the superposition $\tilde{\Theta}_F(t)=\tilde{\Theta}^c_{F,0}(t)+\tilde{\Theta}^c_{F,1}(t)+\tilde{\Theta}^i(t)$.

Fig. 15 shows the power spectral densities of $\Theta(t)$ and $\tilde{\Theta}_F(t)$. The solid line is the average power spectral density of the response $\Theta(t)$ of the system in Eq. (37) to the 11 independent realizations of $M(t)$. The broken line in Fig. 15 is the power spectral density of $\tilde{\Theta}_F(t)$ of the response of Eq. (39). The power spectral densities have two distinct peaks, located at 0.1 and 0.4 Hz, corresponding to the wave force energy content and the oscillator natural frequencies, respectively. There is a good agree-

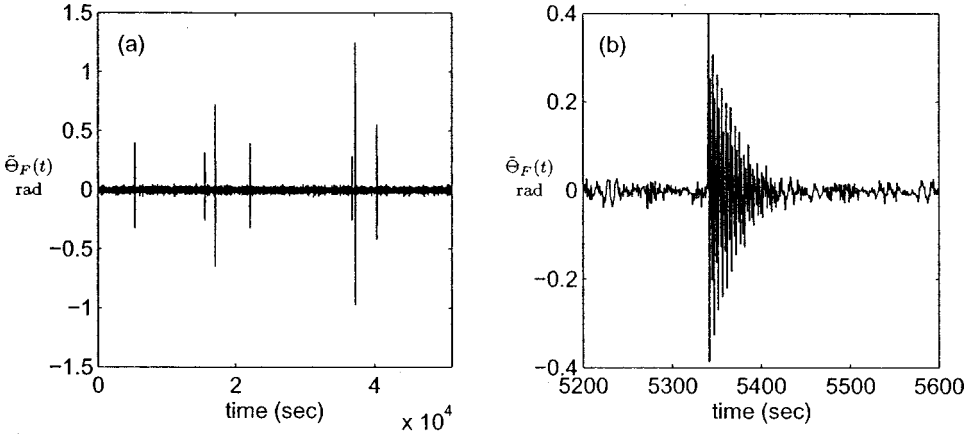

Fig. 14. System response $\tilde{\Theta}_F$ to a sample of $X_F(t)$

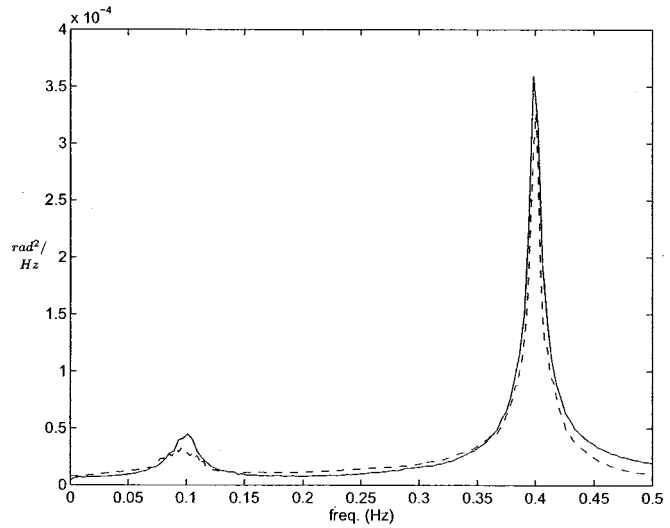

Fig. 15. Power spectral densities of $\Theta(t)$ (solid line) and $\tilde{\Theta}_F(t)$ (broken line)

ment between the response of the system in Eq. (37) to the empirical data and the proposed model.

Estimates of the first four moments are obtained via the Monte Carlo simulation on a single sample 500,000 time steps long ($\delta t = 1$ s). Table 3 summarizes results obtained for the stationary first four moments of the system response $\Theta(t)$ and $\tilde{\Theta}_F(t)$ using the Itô differentiation rule and the Monte Carlo simulation method.

The agreement between the first four moments of the responses $\Theta(t)$ of Eq. (37) and $\tilde{\Theta}_F(t)$ of Eq. (39) is good. In particular, very good agreement is found for the mean, variance, and coefficient of kurtosis. The difference in the coefficient of skewness can be improved by changing to nonsymmetric distributions the impulses $\{Y_{k,0}\}$ and $\{Y_{k,1}\}$.

Conclusions

The response of offshore platforms experience sudden infrequent large-magnitude bursts of short duration referred to as ringing. It is very important that this feature of platform response be considered in the overall design and subsequent performance evaluation of offshore platforms. In this study, two probabilistic models have been used to qualitatively and quantitatively capture the ringing phenomenon. Ringing was simulated using a single-degree-of-freedom oscillating column piercing the water surface. Due to variations in the wetted surface of the column, the moment resulting from the integration of the non-Gaussian wave force is non-Gaussian with infrequent impulses. Two probabilistic models have been developed to describe this non-Gaussian behavior: (i) a translation process superimposed with a Poisson white noise process, and (ii) a filtered Poisson process superimposed with two Poisson white noise processes. Model parameters were estimated from the simulated wave force records. Statistics of the response of an idealized offshore platform represented as a single-degree-of-freedom oscillator to these models and the corresponding records were obtained using the Itô differentiation rule and the Monte Carlo simulation procedure. Good agreement between the results obtained using the two probabilistic wave force models and the records has been found. The use of the second probabilistic wave model with the Itô differentiation rule provides a tool to compute exact moments of any order of the response of single- and multi-degree-of-freedom linear structures to this wave force model. The probabilistic framework presented here would serve as a building block for examining the ringing observed in large volume offshore platforms utilizing more refined hydrodynamic and/or structural models.

Table 3. Stationary Response Moments for the Poisson Model $X_F(t)$

		$\tilde{\Theta}_F(t)$	
Statistics	$\Theta(t)$	Itô Formula	Monte Carlo Simulation
$E[\cdot]$	-8.34×10^{-4}	-0.8×10^{-3}	-3.1×10^{-3}
Var$[\cdot]$	0.0020	0.0020	0.0018
γ_3	0.6772	0.20	0.26
γ_4	88.9081	98	92

Acknowledgments

The support for this work was provided by ONR Grant No. N00014-93-1-0761 and NSF Grants No. CMS 95-03779 and No. CMS 99-84635.

Notation

The following symbols are used in this paper:

a_i, b_i = translational model marginal distribution parameters;
$B(x)$ = beta function;
C_d = drag coefficient;
c = offshore structure damping;
$c_r(t)$ = distance of the center of rotation to the mean water level (m);
D = diameter of a cylindrical column (m);
d = water depth (m);
d_l = length of the discretized section (m);
d_r = draft (m);
$\hat{F}_i(x)$ = empirical marginal distribution of impulse component;
$\tilde{F}_i(x)$ = Weibull cumulative density function;
$F_l(t)$ = cylinder drag force per unit length (N/m);
$\hat{F}_m(x)$ = empirical marginal distribution of the continuous component;
$\tilde{F}_m(x)$ = translational model marginal distribution;
$\hat{F}_\tau(x)$ = empirical marginal distribution of impulses interarrival times;
$F_0(x)$ = student's t cumulative distribution function;
$F_1(x)$ = standard Gaussian cumulative distribution function;
f_0, c_0, f_d = impulse response function parameters;
$\hat{g}$ = power spectral density of the continuous component;
$\tilde{g}$ = power spectral density of a stationary Gaussian process;
$\tilde{g}_{X_T^c}$ = power spectral density of the translation model;
g_0, f_0, ζ_0 = stationary Gaussian process power spectral density parameters;
$h(t)$ = impulse response function;

k = offshore structure stiffness;
M = moment produced by the drag forces on the cylinder $(N-m)$;
$M^c(t)$ = continuous component of input moment $M(t)$ $(N-m)$;
$M^i(t)$ = impulse component of input moment $M(t)$ $(N-m)$;
m = offshore structure moment of inertia;
N = homogeneous Poisson counting process;
na, nb = cylinder segment numbers;
$u(t)$ = water particle velocity (m/s);
$u_i(t)$ = local water velocity at the ith discrete portion of the cylinder (m/s);
$u_{\text{mwl}}(t)$ = water particle velocity at the mean water level (m/s);
$X_F(t)$ = Poisson wave force model $(N-m)$;
$X_F^c(t)$ = continuous component of the Poisson wave force model $(N-m)$;
$X_{F,0}^c(t)$ = filtered Poisson process $(N-m)$;
$X_{F,1}^c(t)$ = Poisson white noise process $(N-m)$;
$X_T(t)$ = translation wave force model $(N-m)$;
$X_T^c(t)$ = continuous component of the translation wave force model $(N-m)$;
$X^i(t)$ = impulse component of the wave force model $(N-m)$;
$Y(t)$ = stationary Gaussian process;
$Z(t)$ = zero mean stationary Gaussian process;
α, c = Weibull distribution parameters;
γ_3 = skewness coefficient of a random variable or process;
γ_4 = kurtosis coefficient of a random variable or process;
Δt = time interval (s);
$\delta(t)$ = delta Dirac function;
$\eta(t)$ = wave elevation with respect to the mean water level (m);
$\Theta(t)$ = system response to $M(t)$ (rad);
$\tilde{\Theta}_F(t)$ = system response to $X_F(t)$ (rad);
$\tilde{\Theta}_F^c(t)$ = system response to $X_F^c(t)$ (rad);
$\Theta^i(t)$ = system response to $X^i(t)$ (rad);
$\tilde{\Theta}_T(t)$ = system response to $X_T(t)$ (rad);
$\tilde{\Theta}_T^c(t)$ = system response to $X_T^c(t)$ (rad);
Λ = impulses arrival time (s);
λ = impulses mean arrival rate (arrivals/s);
μ = mean of a random variable or process;
ν = degree of freedom of the student t distribution;
ρ = fluid density (N/m^2);
σ = standard deviation of a random variable or process;
τ = impulses interarrival times (s); and
$\Phi(x)$ = Gaussian cumulative density function.

References

Chaplin, J., Rainey, R., and Yemm, R. (1997). "Ringing of a vertical cylinder in waves." *J. Fluid Mech.*, 350, 119–147.

Davies, K., Leverette, S., and Spillane, M. (1994). "Ringing of TLP and GBS platforms." *BOSS*.

Faltinsen, O., Newman, J., and Vinje, T. (1995). "Nonlinear wave loads on a slender vertical cylinder." *J. Fluid Mech.*, 289, 179–198.

Gihman, I. I., and Skorohod, A. V. (1972). *Stochastic differential equations*, Springer, New York.

Grigoriu, M. (1995). *Applied non-Gaussian processes: Examples, theory, simulation, linear random vibration, and MATLAB solutions*, Prentice Hall, Englewood Cliffs, N.J.

Gurley, K., and Kareem, A. (1998). "Simulation of ringing in offshore systems under viscous loads." *J. Eng. Mech.*, 124(5), 582–586.

Gurley, K., Kareem, A., and Tognarelli, M. (1996). "Simulation of a class of non-normal processes." *Int. J. Non-Linear Mech.*, 31(5), 601–617.

Hasselmann, K. (1962). "On the nonlinear energy transfer in a gravity wave spectrum, Part I." *J. Fluid Mech.*, 12, 481–500.

Hudspeth, R., and Chen, M. (1979). "Digital simulation of nonlinear random waves." *J. Waterw., Port, Coastal Ocean Div., Am. Soc. Civ. Eng.*, 105(1), 67–85.

Ikeda, N., and Watanabe, S. (1981). *Stochastic differential equations and diffusion processes*, North-Holland, New York.

Jeffreys, E., and Rainey, R. (1994). "Slender body models of TLP and GBS ringing." *BOSS*.

Johnson, N., and Kotz, S. (1970). *Distributions in statistics: Continuous univariate distributions-2*, Houghton Miffin, Boston.

Kareem, A., Hsieh, C., and Tognarelli, M. (1994). "Response analysis of offshore systems to nonlinear random waves Part I: Wave field characteristics." *Proc., Special Symposium on Stochastic Dynamics and Reliability of Nonlinear Ocean Systems*, ASME, Chicago.

Krokstad, J., Stansberg, C., Nestegard, A., and Marthinsen, T. (1998). "New nonslender ringing load approach verified against experiments." *J. Offshore Mech. Arct. Eng.*, 120(1), 20–29.

Matlab (1998). *Matlab Optimization ToolBox*, Mathworks Corporation, Boston, Mass.

Mo, O., and Moan, T. (1985). "Environmental load effect analysis of guyed towers." *J. Energy Resour. Technol.*, 107, 24–33.

Natvig, B. (1994). "A proposed ringing analysis model for higher order tether response." *Proc., 4th Int. Offshore and Polar Engineering Conf.*, Osaka, Japan, 40–51.

Newman, J. (1995). "To second order and beyond." *TLP Technology Symposium*.

Samorodnitsky, G., and Taqqu, M. S. (1994). *Stable non-Gaussian random processes. Stochastic models with infinite variance*, Chapman and Hall, London.

Snyder, D. (1975). *Random point processes*, Wiley, New York.

Snyder, D., and Miller, M. (1991). *Random point processes in time and space*, Springer, New York.

Waisman, F. (1998). "Applications of non-Gaussian models to the solution of structural engineering problems." PhD thesis, Cornell Univ., Ithaca, N.Y.

Waisman, F., and Grigoriu, M. (1998). "Nonlinear systems driven by polynomials of filtered Poisson processes." *Probab. Eng. Mech.*, 14(1–2), 195–203.